Wet deposition in a global size-dependent aerosol transport model 1. Comparison of a I year løpb simulation with ground measurements

W. Guelle, Yves Balkanski, M Schulz, F. Dulac, P Mortfray

JOURNAL OF GEOPHYSICAL RESEARCH, VOL. 103, NO. D10, PAGES 11,429–11,445, MAY 27, 1998

Wet deposition in a global size-dependent aerosol transport model
1. Comparison of a 1 year ^{210}Pb simulation with ground measurements

W. Guelle and Y. J. Balkanski
Laboratoire des Sciences du Climat et de l'Environnement, Direction des Sciences de la Matière, Commissariat à l'Energie Atomique, Gif-sur-Yvette, France

M. Schulz
Institut für Anorganische und Angewandte Chemie, Universität Hamburg, Hamburg, Germany

F. Dulac and P. Monfray
Centre des Faibles Radioactivités, Centre National de la Recherche Scientifique - Commissariat à l'Energie Atomique, Gif-sur-Yvette Cedex, France

Abstract. We present and discuss results from a 1 year (1991) global simulation of the transport and deposition of ^{210}Pb with a new size-resolved aerosol transport model. The model accounts for aerosol size distribution and its evolution during transport. Our wet deposition scheme is size-dependent and distinguishes between scavenging by deep and shallow convective rains. It treats separately below- and in-cloud scavenging by synoptic rains. Although the model is formulated to treat all aerosol sizes, the validation was done for the ^{210}Pb submicronic aerosol for which the main sink is wet deposition. We assess the model transport and deposition of submicron aerosols by a comparison of model results with available surface measurements. Annual mean surface concentrations are compared at 117 stations throughout the globe; seasonal variations are examined for 35 of these sites. The mean bias between simulated and measured yearly averaged surface concentrations is -2.7%, and the correlation coefficient is 0.80. The observed seasonal cycle and the annual mean concentrations are particularly well reproduced, although the model's poor vertical resolution does not capture the strong winter peak at some continental stations, nor the transport to Indian Ocean stations. Using the observed precipitation at or near the sites studied, we were able to explain a large part of the bias in model annual deposition. Deposition at coastal sites deserves also a special treatment since influenced by the land-ocean partition inherent to the model. When we represent correctly these coastal stations, we reduce the mean bias between observed and predicted annual deposition fluxes from 7.7% to 1.2% at 147 stations, and the correlation coefficient improves from 0.70 to 0.77.

1. Introduction

Recently, aerosols have been the focus of research on their link to climate. Radiative forcing studies have tried to document whether aerosol cooling effect could compensate the warming due to anthropogenic greenhouse gases [*Charlson et al.*, 1992; *Penner et al.*, 1992; *Kiehl and Briegleb*, 1993; *Sokolik and Toon*, 1996; *Tegen et al.*, 1996]. These modeling studies rely on the global three-dimensional (3-D) distribution of sulfate aerosol [*Langner and Rodhe*, 1991; *Pham et al.*, 1995; *Feichter et al.*, 1996; *Chin et al.*, 1996], carbonaceous aerosol [*Penner et al.*, 1991; *Cooke and Wilson*, 1996; *Liousse et al.*, 1996], and mineral aerosol [*Joussaume*, 1990; *Genthon*, 1992; *Tegen and Fung*, 1994; *Tegen et al.*, 1996], which are the main constituents responsible for the global aerosol forcing [*International Panel on Climate Change*, 1994]. Our ability to estimate the radiative effect of these aerosols depends mainly on our knowledge of their optical properties and of the accuracy with which we describe their sources and sinks.

Paper number 97JD03680.
0148-0227/98/97JD-03680$09.00

The most important removal process for submicron aerosols is scavenging by precipitation. *Arimoto et al.* [1985] have measured a contribution of the aerosol wet deposition flux to the total deposition flux in the Pacific of 70 to 90% for trace elements, far from their source region. In a rural area, i.e., closer to source areas, *Prakasa Rao et al.* [1992] measured wet deposition flux contributions of 74 and 62% for sulfate and nitrate aerosols, respectively. In regions far from the sources, where the biggest particles have already been removed by gravitational settling, this contribution has been estimated to be 60 to 85% for desert dust [*Arimoto et al.*, 1985; *Uematsu et al.*, 1985; *Dulac et al.*, 1989]. The simulation of wet scavenging is therefore of utmost importance to assess the atmospheric mass load and deposition flux of aerosols.

A comprehensive validation of a wet-scavenging scheme for any aerosol data is hampered, given the paucity of the number of available measurements to compare with model results. To validate aerosol scavenging in global models, authors have compared model results to radionuclide measurements [*Feichter et al.*, 1991; *Lee and Feichter*, 1995]. Lead 210 is the decay daughter of ^{222}Rn of which the source is principally continental origin, with a ground emission rate estimated in the range 0.72-1.2 atom cm^{-2} s^{-1} [*Turekian et al.*, 1977; *Lambert et al.*, 1982]. Compared to other aerosols, the source of ^{210}Pb is relatively well known. Because of its short lifetime (half-life, 3.8 days), most of ^{222}Rn resides in the low troposphere and is used to study rapid vertical exchange between the planetary boundary layer (PBL) and the free troposphere [*Brost and Chatfield*, 1989; *Feichter and Crutzen*, 1990; *Jacob and Prather*, 1990; *Mahowald et al.*, 1995; *Jacob et al.*, 1997]. Hence ^{210}Pb is mainly formed in the low troposphere where it rapidly attaches to ambient particles whose size is essentially less than 1 μm [*Sanak et al.*, 1981; *Knuth et al.*, 1983; *Schneider et al.*, 1983; *Bondietti et al.*, 1987, 1988]. Therefore sedimentation is almost negligible for these particles. *Knuth et al.* [1983] and *Todd and Wong* [1989] have estimated that less than 15% of the total ^{210}Pb deposition flux is due to dry deposition. It is therefore an excellent tracer to focus on the validation of the wet deposition scheme in the model. Moreover, many measurements exist over the whole globe, such as monthly averaged surface air concentrations gathered by the Environmental Measurements Laboratory [*Larsen et al.*, 1995] as well as annual concentrations and deposition fluxes compiled by *Preiss et al.* [1996] in a large database.

We present in this paper a wet deposition scheme in a global 3-D aerosol transport model that we validate against measurements taken during 1991. We focus on the available data for year 1991 since the model is driven by analyzed fields from the European Centre for Medium-Range Weather Forecast (ECMWF) for this year. We also examine climatological concentrations and deposition fluxes. Our wet deposition scheme distinguishes between convective and large-scale precipitation (also called synoptic precipitation), the former occurs more frequently in the tropics, while the latter is more common at middle and high latitudes. In the case of synoptic precipitation we distinguish between in-cloud and below-cloud scavenging. For the latter the dependence on particle size is accounted for. This is important for the scavenging of large aerosols such as mineral dust and sea salt. We describe afterward the ability of the model to simulate the observed concentrations and deposition fluxes measured at more than a hundred different sites throughout the world. The discussion includes sensitivity studies on the parameters controlling the different mechanisms involved in our parameterization of the wet scavenging of aerosols.

2. Model Description

2.1. General

This study uses the three-dimensional atmospheric model of tracer transport TM2 developed by Martin Heimann at the Max-Planck-Institut für Meteorologie in Hamburg [*Heimann and Keeling*, 1989; *Heimann*, 1995]. It is an "off-line" model that can be driven by ECMWF-analyzed fields. Advection is treated following the method of *Russell and Lerner* [1981], with a slope limitation added to avoid negative concentrations. Sub-grid-scale vertical exchange processes are formulated using the *Louis* [1979] parameterization for turbulent vertical transport and a simplified version of the *Tiedtke* [1989] scheme to compute the mass fluxes in cumulus clouds (from the 12 hourly ECMWF fields of geopotential, surface pressure, horizontal wind, temperature, relative humidity, and surface evaporation fluxes).

We use a high-resolution version of the transport model (2.5°×2.5°) with nine sigma levels extending from the ground level to 10 mbar, six to eight of them describing the troposphere depending on latitude [*Ramonet*, 1994]. The 12 hourly ECMWF 3-D analyzed wind fields of 1991 are interpolated on these nine layers during the preprocessing stage and used as input to the model. Each of the transport and deposition processes is computed with a 1 hour time step.

In a previous work, *Schulz et al.* [1997] have incorporated an aerosol transport module in the TM2 which allows the model to reproduce the change of the aerosol size distribution during transport. This scheme partitions the aerosol mass loading among one to several modes, each of them being represented by a lognormal function whose parameters are mass median diameter (MMD) (or number median diameter (NMD)) and geometric standard deviation σ. In our simulation we have set the size distribution parameters of ambient aerosol to which ^{210}Pb attaches to 0.4 μm for the MMD and 1.9 for σ according to measurements made by *Bondietti et al.* [1987]. This yields a NMD of about 0.12 μm. Once ^{210}Pb attached to particles,

the MMD is recomputed at each location and each time step. For the source, we used the global 3-D distribution of monthly averaged concentrations of ^{222}Rn archived from a previous simulation of year 1991 with the same model [*Ramonet and Monfray,* 1996]. A constant emission flux of 1 atom cm^{-2} s^{-1} over continental areas had been adopted, which lies in the observed range of global mean estimations [*Turekian et al.,* 1977; *Lambert et al.,* 1982]. The continental fraction of each model grid boxes was computed from a 0.7° longitude × 0.35° latitude data bank to exclude oceanic emissions. Emissions from Greenland and Antarctica were also excluded since ice cover prevents them [*Wilkening and Clements,* 1975; *Lambert et al.,* 1982]. Turbulent deposition in the lowest model layer is simply computed here using constant dry deposition velocities. The velocities used are global averages computed by *Balkanski et al.* [1993]: 0.05 cm s^{-1} over oceans and 0.2 cm s^{-1} over land. Since the dry deposition is only responsible for a small fraction ($\leq$ 15%) of the total deposition flux on a global scale [*Knuth et al.,* 1983; *Todd and Wong,* 1989], this simple parameterization is satisfying over most of the globe. In dry areas, such as those in subtropical and polar regions, we could be underestimating dry deposition.

2.2. Wet Deposition

The wet deposition scheme described here distinguishes between convective and large-scale precipitation. In a convective event, resulting from the large-scale convergence of moist air, the latter is entrained through the base and the sides of the convective cloud, and while climbing and condensating will give birth to precipitation of short duration and great intensity. Aerosol particles present near the cloud are entrained inside these strong updrafts, a part of them being scavenged by the accompanying formation of precipitation. *Balkanski et al.* [1993] pointed out the importance of these rapid vertical exchanges of aerosols to determine the fraction of aerosols scavenged from the one redistributed outside from the cloud.

In the case of synoptic rain, total evaporation below the cloud base can release aerosols in the lowest levels, but it does not modify the vertical distribution of the aerosols as much as in the case of cloud convection. Hence we chose to use a first-order removal scheme to treat scavenging by synoptic precipitation. Different processes account for aerosol scavenging by synoptic rain in and below the precipitating cloud. For in-cloud scavenging, aerosol particles act as cloud condensation nuclei. We considered that all the aerosol in the cloud is incorporated in cloud droplets. For below-cloud scavenging we compute washout of aerosol by falling raindrops according to both the precipitation rate and the particle size. We assume here that scavenging by snow occurs with the same efficiency as rainwater.

2.2.1. Scavenging by convective precipitation. Following *Balkanski et al.* [1993] we compute aerosol scavenging in convective precipitation as part of the mass flux entrained in convective cloud. We distinguish between shallow wet convective events extending up to the third level of the model ($\sim$ 2.6 km) and deep wet convection extending to higher levels. The aerosol mass entrained in the updrafts can be retrieved from the *Tiedtke* [1989] scheme used to describe the convection in the model. We scavenge 100% of the aerosol pumped in deep wet convection events and 50% in wet shallow convection events according to the sensitivity studies of *Balkanski et al.* [1993]. The scavenging is computed hourly whenever convective rain occurs, as determined by the 12 hourly ECMWF 24 hour forecasts of ground convective precipitation rates.

2.2.2. In-cloud scavenging by synoptic precipitation. In-cloud scavenging of the aerosol is treated following *Giorgi and Chameides* [1986] parameterization; the reader will find the details of the implementation in the *Balkanski et al.* [1993]. The ECMWF only provides precipitation rates at the ground and not precipitation formation aloft. To derive the precipitation aloft, we used the climatological 5 day mean condensation rate from the Goddard Institute for Space Studies (GISS) general circulation model (GCM) averaged zonally over 4° wide bands. These profiles were interpolated onto the model grid and normalized to the ground synoptic precipitation rate provided by ECMWF through its 12 hourly 24 hour forecasts. This vertical distribution probably induces biases in our simulation since it is not accounting for any interannual variation between this climatological year and the year 1991, nor do we account for variations between continental and marine profiles. Unfortunately, we have no other such information to determine the extent to which these simplifications affect our results. For each layer, according to the rain rate difference between upper and lower boundaries, we compute in-cloud scavenging when there is rain formation. All small particles such as ^{210}Pb carriers in the cloud are assumed to be incorporated in the liquid phase, hence the aerosol is removed with this scheme as cloud water.

2.2.3. Below-cloud scavenging by synoptic precipitation. In the case where there is no rain formation in the grid box but precipitation occurs, we compute below-cloud scavenging using the area fraction computed in the lowest level where rain is formed. We assume partial evaporation to result in a reduction of the size of the raindrops containing particles rather than total evaporation of some raindrops. Therefore we assume a perfect retention of particles once incorporated by raindrops. Since our model is driven by ground precipitation rates and 5 day averaged vertical distributions of rain, local cases of total evaporation (implying resuspension of particles) do not occur.

For below-cloud scavenging we must account for the selective removal of aerosol according to their size and to the raindrop size distribution. We use *Dana and Hales* [1976] parameterization which requires only aer-

osol and raindrop size distributions (hereinafter referred to as ASD and DSD, respectively) as well as the rainfall rate. *Dana and Hales* [1976] assume a lognormal distribution for the raindrop size distribution characterized by a geometric mean diameter equal to 400 μm and a geometric standard deviation of 1.86 and assumed it invariant with time and altitude. Integrating the collection efficiency over the whole raindrop size distribution gives the washout coefficient $\lambda^*(d, \mathrm{DSD})$ for a single particle of diameter d (see appendix for definition of λ^*, Λ^*, and η). We integrate $\lambda^*(d, \mathrm{DSD})$ over the aerosol size distribution (see appendix for calculation details) to obtain the scavenging efficiency for the whole aerosol. Much uncertainty exists on the value of λ^*. Particularly *Schumann* [1989] has measured in situ a mean λ^* value 20 times greater than the one we compute for ^{210}Pb characteristics. The importance of this discrepancy will be evaluated in section 5.

3. Simulation Results for 1991

We have performed a 3-D global simulation of ^{210}Pb for 14 months beginning November 1, 1990, and analyzed solely the last 12 months to ensure that ^{210}Pb tropospheric concentrations were close to steady state. The production rate of ^{210}Pb in our model is 13.8 kg yr^{-1}. Figures 1a-1d show the global distribution of ^{210}Pb concentrations for January and July 1991, both in surface air and at $\sim$ 6 km altitude in the model. Highest concentrations are found over continents near the surface where ^{222}Rn (from which ^{210}Pb is formed) is most abundant. These figures exhibit a strong north-to-south latitudinal gradient because about 37% of the northern hemisphere is covered by continents (excluding the permanently frozen Greenland) versus 16% for the southern hemisphere (excluding Antarctica).

These figures illustrate the ability of our model to reproduce well-known features of atmospheric transport. During January the boundary layer transport of Asian aerosol to North America is well simulated. This phenomenon, called Arctic haze, is produced by a winter southward movement of the polar front to the midlatitudes, allowing Asian aerosol to reach polar latitudes and then North America since little precipitation occurs on this transport pathway at this time of the year [*Rahn and McCaffrey,* 1980].

Another important large-scale pattern that is well simulated by the model is the seasonal shift of the Intertropical Convergence Zone (ITCZ). In winter it is located between 10°S and 10°N, whereas in summer, it shifts northward between 0°N and 20°N. The model predicts January concentrations greater than 1000 μBq m^{-3} over entire India, whereas in July, when the ITCZ is located northward over the Asian continent, the strong monsoon precipitation scavenging decreases concentrations below 500 μBq m^{-3}. The effect of the ITCZ is even more pronounced over the North Atlantic: in winter the aerosol plume coming from North Africa is transported by the trade winds to the Amazon Basin, whereas in summer, the ITCZ pushes this plume north-

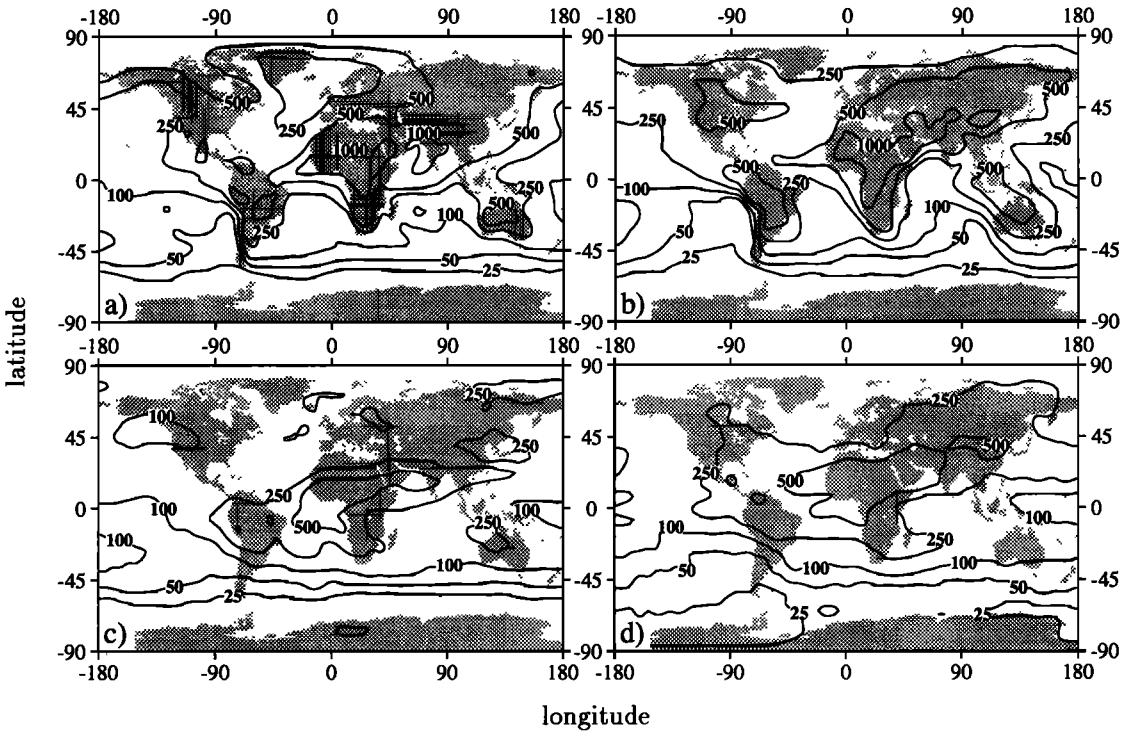

Figure 1. Simulated ^{210}Pb concentration (μBq m^{-3}) for 1991 in surface air for (a) January and (b) July, and at $\sim$ 6 km altitude for (c) January and (d) July. Isolines are 25, 50, 100, 250, 500, and 1000.

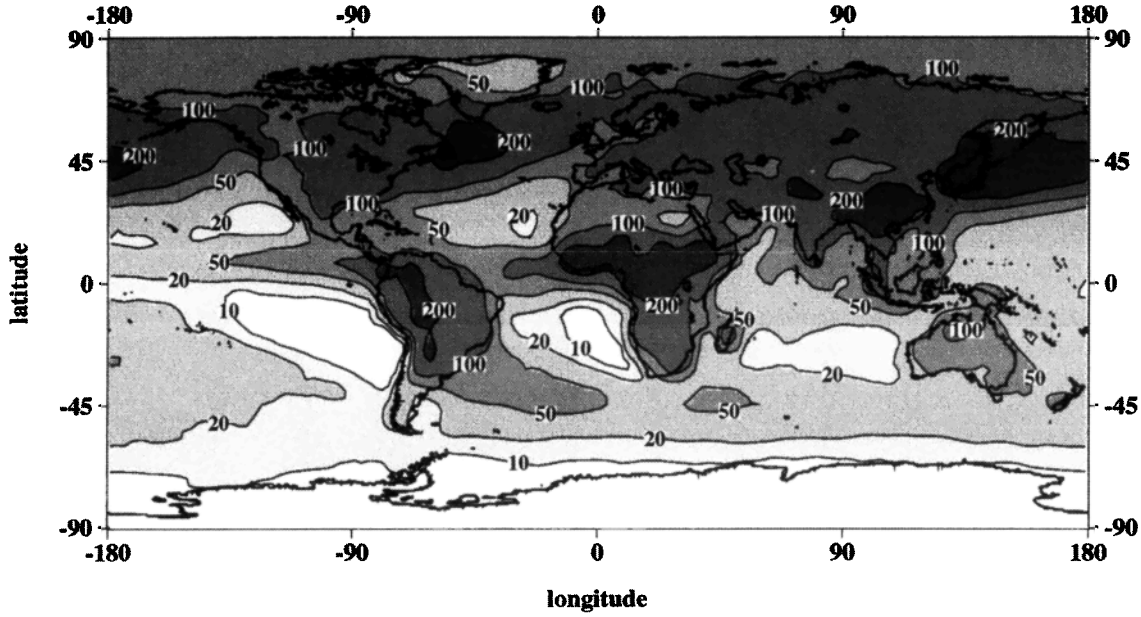

Figure 2. Simulated annual total deposition flux of ^{210}Pb (Bq m^{-2} yr^{-1}). Isolines are 10, 20, 50, 100, and 200.

ward toward the Carribean Sea. This shift can also be seen on satellite images [*Husar et al.*, 1997] where the signal is dominated by mineral aerosol originating from Sahara.

The model reproduces also some characteristic patterns of vertical distribution of aerosols with transport in higher altitude in July due to a stronger convection in the subtropics. Comparison among Figures 1a-1d shows that transport of African aerosol over the Atlantic takes place at higher levels in July than in January, when most of aerosol is transported near the ground, as shown in the observations [*Chiapello et al.*, 1995]. The same seasonality in transport height can be seen over the western part of the Indian and Pacific Oceans, although to a lesser extent, and has been documented by *Kritz et al.* [1990].

Figure 2 shows the global distribution of annual total ^{210}Pb deposition to the surface. The largest values are found in the northern hemisphere. Over oceans the greater deposition fluxes are downwind from continents at midlatitudes (east coasts) and in the tropics (west coasts). The ^{210}Pb enrichment of marine air flowing over continents enhances this west-east contrast.

Dry deposition contributes to about 15% of total deposition in the model. Figure 3 shows the meridional repartition of zonal mean annual ^{210}Pb flux from dry deposition, and wet scavenging by synoptic and convective precipitation. In our simulation, wet deposition by convective precipitation accounts for 47% of the total global deposition and scavenging by large-scale precipitation for 38%, with less than 1% due to below-cloud scavenging. This balance is intermediate between the one estimated by *Balkanski et al.* [1993] for which scavenging by convective rain is the most important removal process (convective, 74%; synoptic, 12%) and the one estimated by *Feichter et al.* [1991] for which removal is essentially due to large-scale precipitation (convective, 26%; synoptic, 61%).

The mean annual tropospheric scavenging constants (as defined by *Lambert et al.* [1982]) for both hemispheres measure the efficiency with which the aerosol is scavenged. As *Ehhalt* [1973] has shown with ^{137}Cs aerosol, residence time of submicronic aerosol is less than 2 days, on average, in the boundary layer and rises from 5 to 25 days from 2 to 10 km altitude. We found values, in term of mean tropospheric residence time, of 6.6 days for the northern hemisphere and 8.8 days for the southern hemisphere, which are in very good agreement with the 5.9 and 8.8 days values estimated by *Lambert et al.* [1982]. For the global troposphere we

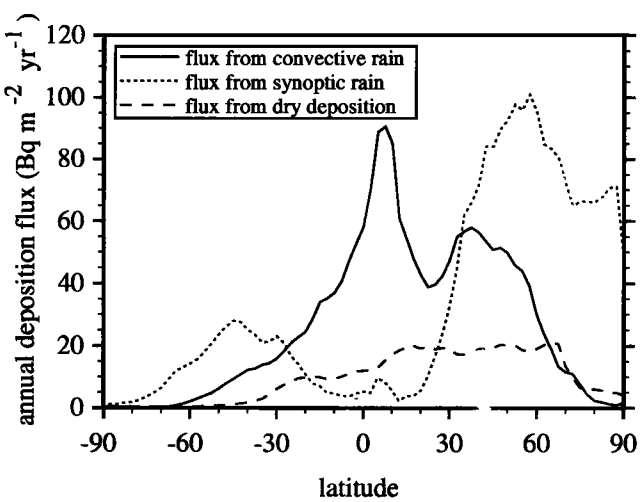

Figure 3. Zonally averaged annual deposition flux of ^{210}Pb (Bq m^{-2} yr^{-1}) due to convective rain, synoptic rain, and dry deposition.

found a mean residence time of 7.2 days in exact agreement with what *Turekian et al.* [1977] have estimated and comparable to 6.5 days estimated by *Lambert et al.* [1982].

4. Validation

4.1. Observational Database

The principal interest in using ^{210}Pb aerosol to validate a global atmospheric model is the very good spatial and temporal coverage of the available measurements. We have considered annual ^{210}Pb surface air concentration measurements at 117 stations and annual ^{210}Pb total deposition flux measurements at 147 stations. Figures 4a-4b locate the stations from which ^{210}Pb measurements are used in this work, and Table 1 gives a summary. *Preiss et al.* [1996] give a summary of the way the measurements are carried out. Sites where concentrations were measured are unevenly distributed but cover all latitudes of the globe. Continental coverage is satisfactory except that we miss data over Russia, China, Middle East, and Central Africa (Figure 4a).

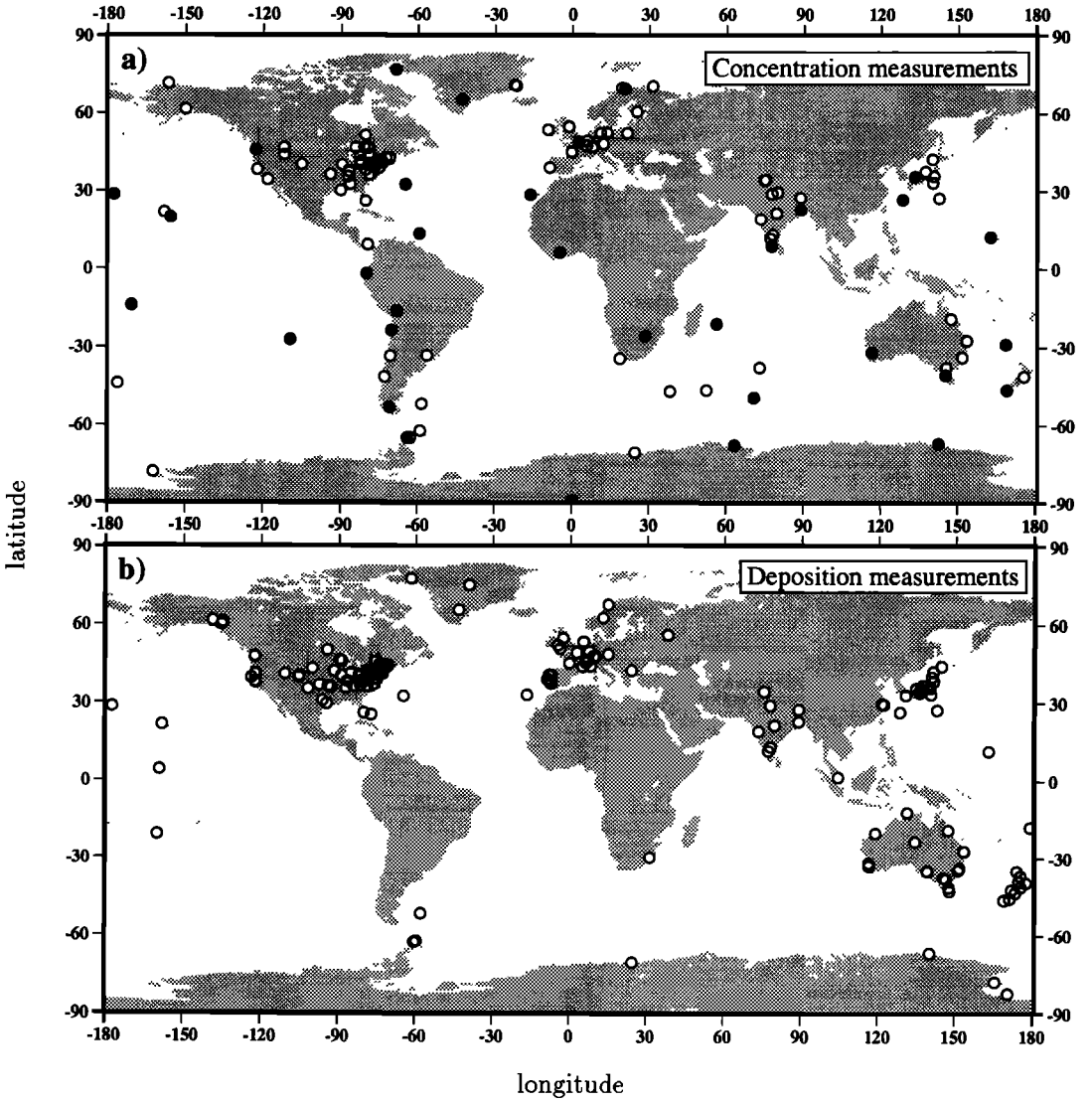

Figure 4. Location of (a) 117 stations measuring annual surface air concentration of ^{210}Pb and (b) 147 stations measuring annual total deposition flux of ^{210}Pb used to validate the model. Solid circles indicate the stations for which monthly concentrations are provided and used in this work. Concentration data used for 1991 are reported by *Larsen et al.* [1995], by *Nho et al.* [1996] for Lamto (Ivory Coast), and from *Centre des Faibles Radioactivités* (CFR) database for Dumont d'Urville (Antarctica). For the averaged measurements, data are from *Tsunogai et al.* [1988] for Japanese stations, as referenced by *Balkanski et al.* [1993] for North Atlantic and North Pacific stations, from *Gopalakrishnan et al.* [1973] for Indian stations, from *Kolb* [1984, 1986, 1988, 1990] for Skibotn (Norway), and from *Commissariat à l'Energie Atomique* (CEA) [1990] for Orsay (France). All the deposition flux measurements are reported by *Preiss et al.* [1996] except those from Japan [*Tsunogai et al.*, 1985], those from North Pacific islands [*Turekian et al.*, 1989], and those carried out at Chester, New Jersey [*Knuth et al.*, 1983].

Table 1. Number of Stations per Region Used for Comparison Between Observed and Modeled Annual Surface Air Concentrations and Total Deposition Fluxes of ^{210}Pb

Region	Surface Air Concentration	Deposition Flux
Greenland	4	3
North America	33	52
Europe	16	25
Japan	7	14
India	11	8
China, Malaysia	...	3
Africa	3	1
Atlantic Ocean	3	3
Pacific Ocean	8	6
Indian Ocean	5	...
South America	11	1
Australia	6	16
New Zealand	2	9
Antarctica	8	6
Global	117	147

Stations recording deposition data are more scattered. In particular, no data are available in South America, and measurements in oceanic regions are scarce (Figure 4b). Nonetheless, there is at least one representative station for both concentration and deposition in each 10° wide latitudinal band. For the stations where we miss measurements for year 1991, we have used data for another year, or a mean over several years when possible. This could bias the comparison with model results for a particular year, since ^{210}Pb concentrations are found to vary from year to year by as much as a factor of 3. This is also true for annual ^{210}Pb deposition, such as in India [*Joshi et al.*, 1969].

4.2. Comparison of Model Results With Monthly Surface Air Concentrations

In order to evaluate the ability of the model to simulate the seasonality of aerosol transport and removal we compared the monthly averaged surface air concentrations of ^{210}Pb observed at some sites with those simulated by the model. Thirty-five stations were chosen to provide a good coverage of the entire globe (solid circles in Figure 4a). As the simulation was done for 1991, we consider measurements made for that year when available, else we use multiyear averages. Figure 5 shows observed and modeled monthly mean concentrations at each station.

4.2.1. Northern high latitudes. At high northern latitudes the model reproduces well the ^{210}Pb concentrations at Dye 3 but not so well at Thule where the simulated seasonal cycle is too weak, although the winter maximum is captured by the model. The deficiency of the model to describe accurately the boundary layer transport is likely to be responsible for the underprediction of wintertime concentrations. The model overestimates the summer concentrations by a factor of 2 at Thule. As stated by *Rehfeld and Heimann* [1995], several deficiencies in the model dynamics could be responsible for such a discrepancy, but we cannot indicate the most important.

For Scandinavian stations such as Skibotn the model does not reproduce the observed spring minimum both in ^{222}Rn and in ^{210}Pb concentrations. *Mattson* [1970] argued that this minimum could be due to a clogging of the soil pores consecutive to a change in the groundwater level due to the thawing of the ground frost. Not accounting for this kind of seasonal change of surface properties at high latitudes in the ^{222}Rn simulation prevents us from an accurate estimate of the ^{210}Pb source and concentrations.

4.2.2. Northern midlatitudes. For continental stations located at northern midlatitudes, such as in North America and Europe, the model reproduces very well the concentrations in summer but underpredicts them in winter. The winter maximum is the result of the boundary layer stratification which causes a strong negative concentration gradient with height close to the ground. The first layer mean height in the model is 400 m, and hence this stratification and its diurnal variation cannot be well reproduced.

For oceanic stations at the same latitudes this problem vanishes because of remoteness of continental sources. Over the North Pacific the model reproduces very accurately the winter maximum and summer minimum at Japanese stations located near the east coast of Asia. Aside from Mauna Loa which is an elevated site, agreement with observations is almost perfect. For North Atlantic stations the maximum concentrations due to advection of ^{210}Pb-rich Saharan air are well reproduced in summer, as in Izaña (2360 m in altitude) and Barbados. The late spring maximum at Barbados is not well simulated, but the weak seasonality at Mace Head and Bermuda is well reproduced.

4.2.3. Tropical latitudes. In tropical regions the winter maximum and summer minimum due to the northward shift of ITCZ is visible both in the observations and in the simulation over India and the Ivory Coast. However, we can notice that the seasonal cycle is much better simulated at Thumba than at Calcutta (both in India). In South America the late-autumn to early-winter maximum is well reproduced at Guayaquil, Ecuador, and Punta Arenas, Chile, which are located north and south of the Andes Cordillera but not at Antofagasta, Chile.

4.2.4. Southern middle and high latitudes. At Kerguelen Island in the Indian Ocean, all simulations of ^{210}Pb with different models, including ours, show a strong overprediction of the yearly averaged concentration, with values of about 40 μBq m^{-3} for the GISS [*Balkanski et al.*, 1993] and ECHAM [*Feichter et al.*, 1991] models and ranging from 50 to 100 μBq m^{-3} for the TM2 model [*Lee and Feichter*, 1995; this work], whereas the observed one is only 10 μBq m^{-3}. *Polian et al.* [1986] showed that ^{222}Rn profiles at Kerguelen increase with altitude in the free troposphere, indicating that trans-

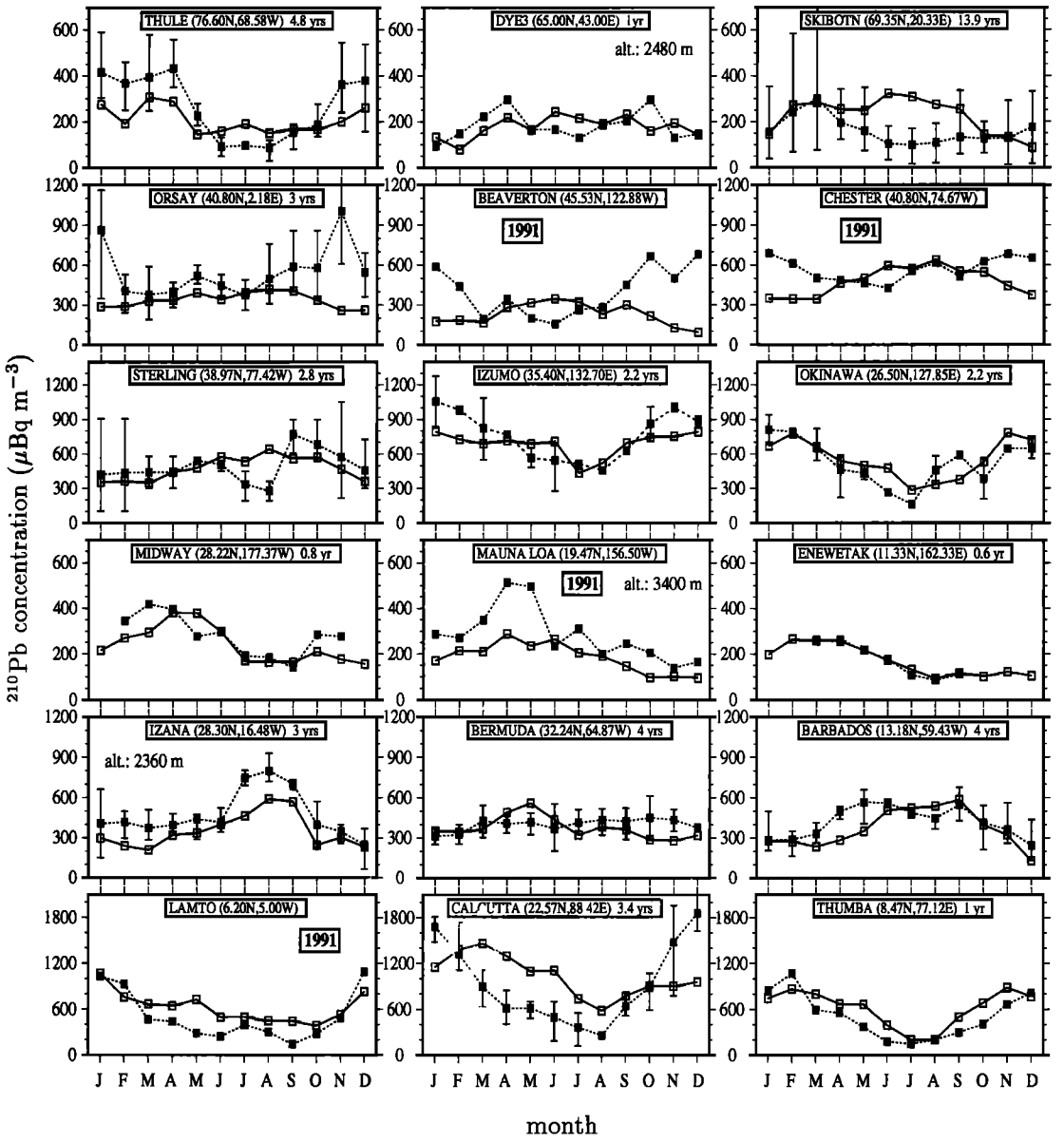

Figure 5. Comparison between observed (solid squares) and modeled (open squares) monthly ^{210}Pb concentration in surface air (μBq m^{-3}) at 35 stations. A label 1991 indicates that measurements have been carried out the same year as the simulation. For measurements not corresponding to year 1991, monthly observed concentrations are averages for which the number of years of data used is indicated, as well as vertical bars corresponding to minimum and maximum values.

port of continental air from South Africa to southern Indian Ocean islands and Antarctica takes place in the middle/upper troposphere (1.5-5 km) rather than at the surface, as seen in the model. It could indicate that the boundary layer over the region is more strongly decoupled from the free troposphere than simulated in the model.

This deficiency of the model to reproduce transport over Indian Ocean has also consequences over Antarctica. At Mawson and Dumont d'Urville the predicted concentrations do not reproduce the summer maximum due to ^{210}Pb-rich air transport in the middle/upper troposphere from the remote continent which subsides over Antarctica [*Polian et al.*, 1986; *Lambert et al.*, 1990]. Everywhere else in the southern hemisphere, our model reproduces very nicely the concentrations and not only on a seasonal scale but also on a monthly scale.

4.3. Comparison of Model Results With Annual Surface Air Concentrations

Figure 6 plots annual mean ^{210}Pb concentrations in surface air issued from the simulation versus those observed. We distinguish between marine and continental stations as well as stations located at latitudes higher than ±45°. For high latitudes the points are more scattered than for the area between 45°N and 45°S. For the northern high latitudes (top panel) the model overestimates the surface concentrations at Canadian sta-

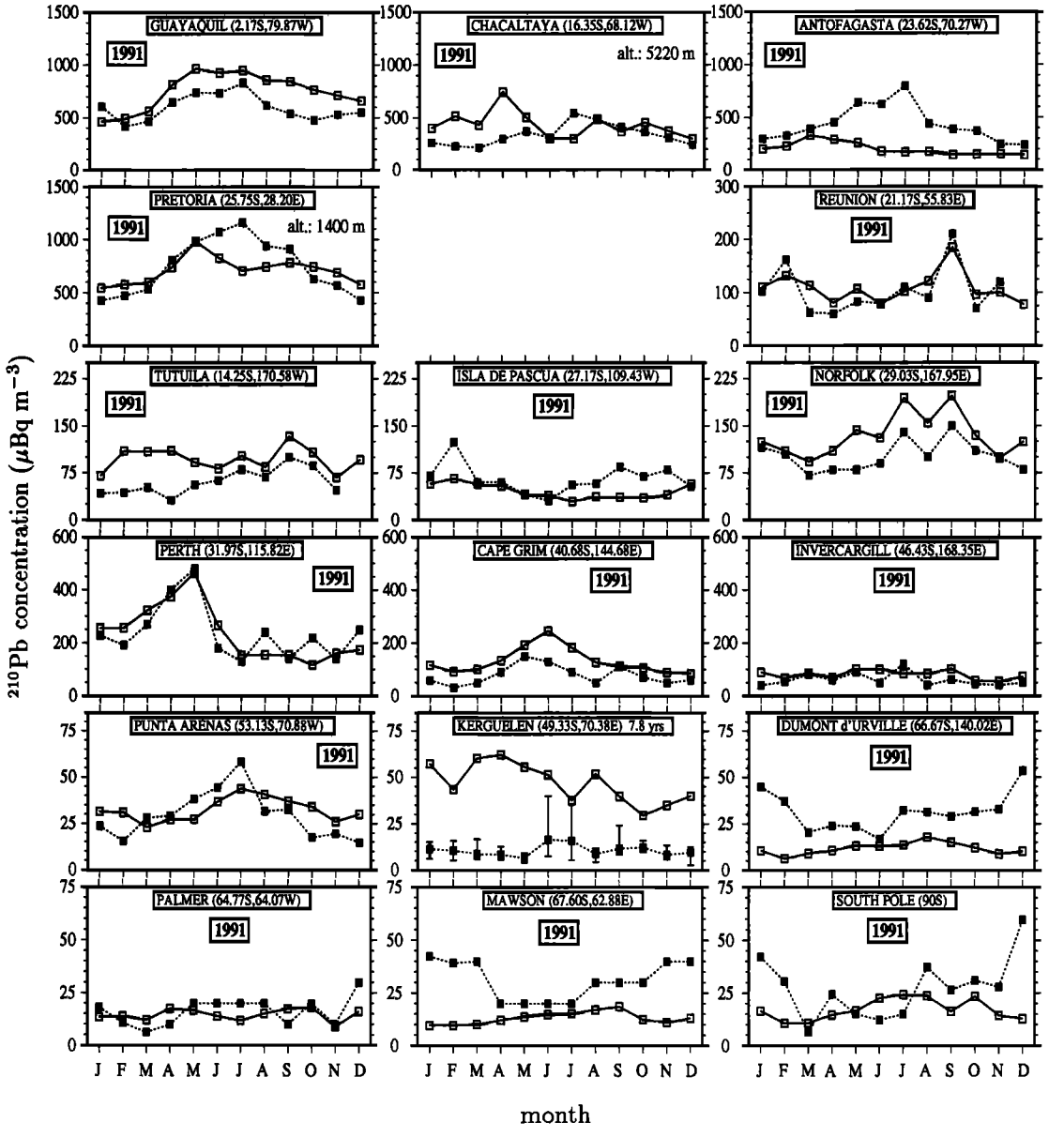

Figure 5. (continued)

tions along the edge of the Great Lakes and underestimates them in Greenland, Europe, and the United States. This underprediction can also be seen at some stations located lower than 45°N. This is likely due to the vertical resolution of the model which does not allow to capture the dynamics of the boundary layer, as discussed in the previous section.

We can notice on Figure 6 the better agreement obtained for all marine stations (squares), except the Indian oceanic islands (bottom), than for continental stations. Marine stations are located far from continents and then are not subject to local fluctuations of ^{222}Rn emission and resulting ^{210}Pb formation. For continental stations, ^{210}Pb concentrations may be influenced by local ^{222}Rn emission variations such as those due to soil freezing, soil water content variations, or different soil types [*Dörr and Münnich,* 1990]. With a constant ^{222}Rn emission rate we are not able to capture these possible variations in ^{222}Rn and ^{210}Pb near ground concentrations. Modeling these effects accurately has yet to be done and beyond the understanding we have of the relationship between ^{222}Rn emanation and soil water content or soil type. Despite these local discrepancies the predicted ^{210}Pb concentrations agree well with the measurements since, globally, the correlation coefficient for all the yearly concentrations is 0.80, with a negligible mean bias equal to -2.7% (for a given station, bias=(value$_{mod.}$−value$_{obs.}$)/max(value$_{mod.}$,value$_{obs}$)).

4.4. Comparison of Model Results With Annual Deposition Fluxes

4.4.1. Flux normalization by observed rainfall rate. Since the annual concentrations are relatively well simulated, we turn now to ^{210}Pb deposition mea-

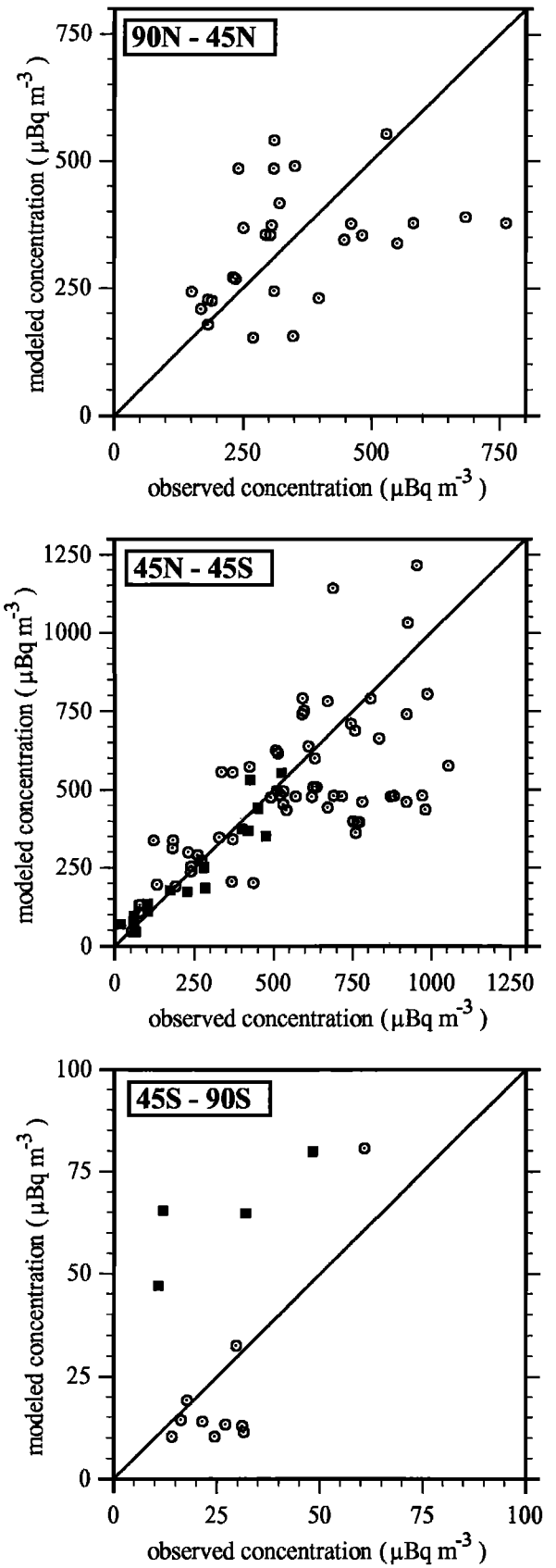

Figure 6. Comparison between observed and modeled annual surface air concentrations of ^{210}Pb (μBq m^{-3}) for the latitudinal bands 90°N-45°N, 45°N-45°S, 45°S-90°S. Dotted circles are for continental stations, and squares for marine stations. The 1:1 lines are also shown.

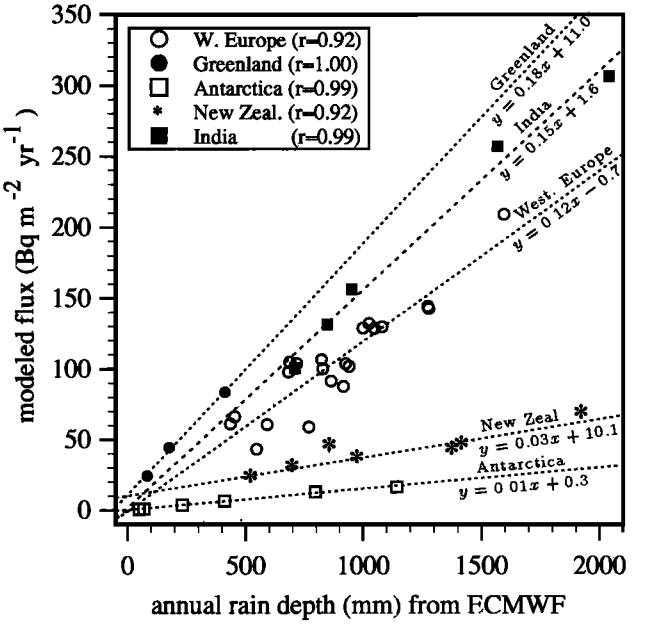

Figure 7. Simulated annual total deposition fluxes of ^{210}Pb (Bq m^{-2} yr^{-1}) versus annual rainfall rate (mm yr^{-1}) for different regions. The correlation coefficient r and the regression lines are indicated.

surements. For this purpose we compared the yearly fluxes simulated with observations at 147 stations. Since most of the deposition is contributed by wet scavenging, it is important to have an accurate description of both the ^{210}Pb atmospheric content and the precipitation rate. We have compared the annual precipitation rates provided by ECMWF at each grid box containing a station with either the one observed by the authors of ^{210}Pb flux measurements at this station or the climatological data from the NOAA Climatological Baseline Station Data over Land, or from *Preiss et al.* [1996] who used a monthly averaged precipitation database with a 30' horizontal resolution. This has revealed that for more than a third of the 147 stations, observed and 2.5°×2.5° averaged ECMWF annual rain rate differ by more than 30%. The ECMWF rainfall rates are representative of the rain amount averaged over a grid box (of roughly 300 km × 300 km near the equator) and not of any particular point within this grid box. Therefore even if our simulated flux represents well the mean flux over the grid box, it may differ significantly from the observed flux at specific stations. In order to shake off this problem we have decided, before comparing our simulated fluxes with the observed ones, to apply a normalization based on both the yearly rainfall rate observed at the measurement site and on the one provided by ECMWF for the 2.5° wide corresponding grid box.

Figure 7 shows the predicted yearly deposition fluxes versus corresponding ECMWF yearly rainfall rate for some stations identifying characteristic regions (not all the regions have been plotted to avoid overlapping points). We can notice that for stations located

in the same region and exposed to similar meteorological conditions and ^{210}Pb atmospheric contents the predicted flux correlates remarkably with the rainfall rate. Different values for the slopes of the straight lines drawn according to specific regions denote different mixing of scavenging processes and/or different ^{210}Pb atmospheric concentrations. It is clear that physically, deposition rates are not linearly dependent on rainfall amounts. Figure 7 shows that considering a given region with a certain regime of precipitation, the predicted deposition flux can be expressed as a linear function of the rainfall rate on an annual timescale and in first approximation. If we consider monthly instead of yearly averages, the correlation coefficients between deposition fluxes and rainfall amounts are significantly reduced from 0.92 to 0.84 for New Zealand, from 0.92 to 0.76 for western Europe, and from 0.99 to 0.74 for India. There is no correlation between deposition and rainfall rates when averaging is done over weekly or daily time periods. We therefore chose to study the simulated fluxes normalized by the ratio of observed and ECMWF rainfall rates:

$$Fx_{\text{normalized}} = \left(\frac{R_{\text{observ}}}{R_{\text{ecmwf}}}\right) Fx_{\text{modeled}}, \qquad (1)$$

with Fx and R being the annual deposition flux and rainfall rate.

Figure 8 presents the simulated versus observed fluxes before and after this normalization by the rainfall rate, at all the stations (102) where the discrepancy between observed and ECMWF annual rainfall rate is greater than 15%. This threshold was chosen in order to see a significant influence in the agreement with observed fluxes. The normalization leads to a noticeable improvement of the simulated fluxes. Indeed, the mean bias for these 102 stations is decreased from 8.4% to 0.9%, and the correlation coefficient is increased from 0.71 to 0.77.

In some instances this normalization does not improve agreement with observations. For the 17 stations where the annual rainfall rate is due to convective precipitation for more than 75%, the mean bias declines from -4.6% to -10.8%, and the correlation coefficient decreases from 0.77 to 0.41 after the normalization. These stations are located in the Pacific and in regions under monsoon influence, such as Japan and India. For these cases a comparison with measurements that have not been carried out the same year than for the simulation is very uncertain. Indeed, we use a climatological value for the annual precipitation rate which can differ from a factor of 2 or greater from the actual one, due to its strong interannual variability. Moreover, measurements have shown that from one year to another, deposition can vary by a factor of 2 for the same annual rainfall amount [*Joshi et al.*, 1969]. It is therefore important to compare observations and simulation results for the same meteorological year to draw any conclusion in these regions.

4.4.2. Flux correction by grid box selection. Another concern when comparing observed and modeled fluxes arises from the model resolution. At coastal stations under marine atmospheric influence, air masses are poor in ^{210}Pb. Lead 210 fluxes at these stations are thus smaller than for inland sites. If the grid box containing the coastal station is mainly covered by continent, its concentration is affected by the local ^{222}Rn source and is thus not representative of the marine air that influences the station most of the time. We therefore chose for coastal stations, located in a grid box in which the continental fraction is greater than 50%, the flux in the nearest grid box for which the oceanic fraction is predominant. At every continental, oceanic, or coastal station located at the border between 2 or 4 grid boxes we also corrected the flux by averaging it over these boxes. Figure 9 plots the simulated versus observed fluxes for the 33 concerned stations. We see

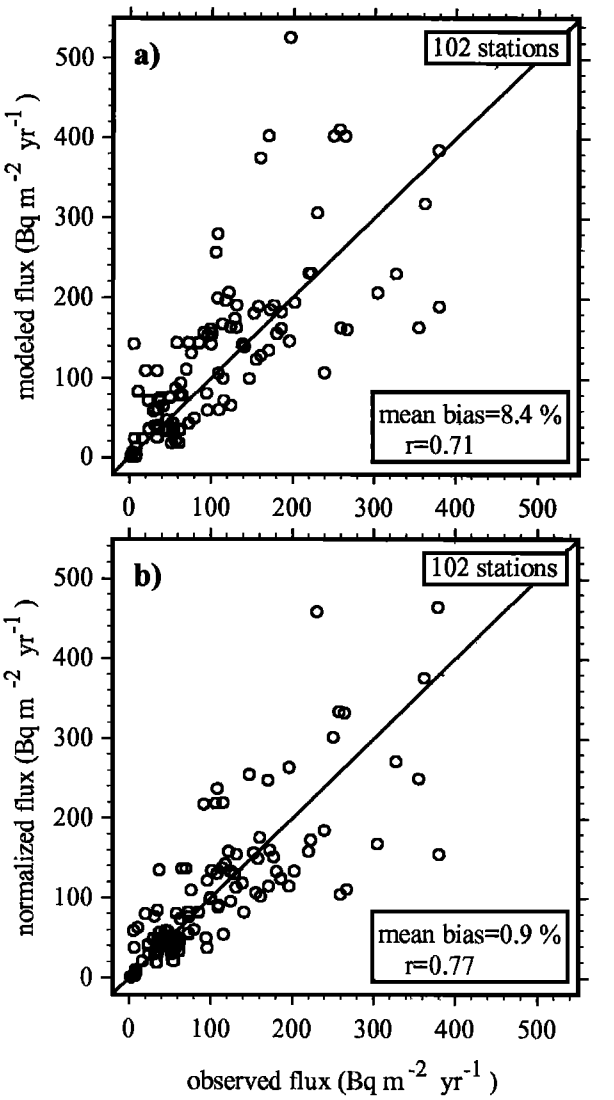

Figure 8. Comparison between observed and modeled annual total deposition flux of ^{210}Pb (Bq m^{-2} yr^{-1}) (a) before and (b) after rainfall rate normalization (see text) at the 102 stations where the difference between observed and ECMWF annual rainfall rate is greater than 15%. The 1:1 lines are also shown.

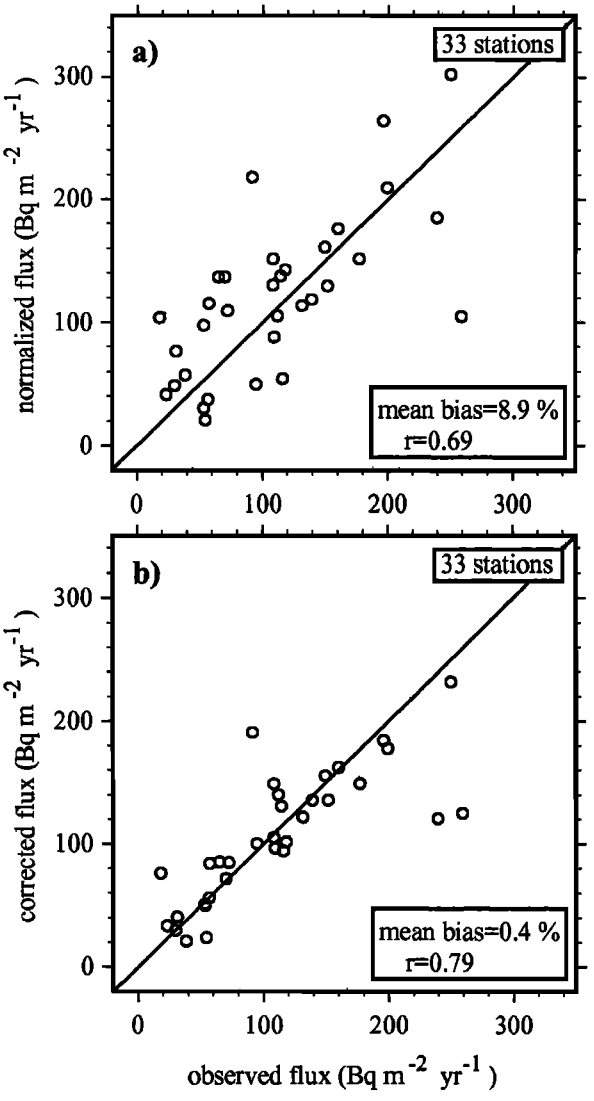

Figure 9. Comparison between observed and modeled annual total deposition flux of ^{210}Pb (Bq m^{-2} yr^{-1}) normalized by observed rainfall rate (a) before and (b) after geographical corrections (see text) at the 33 stations located on the coast or on the border between grid boxes. The 1:1 lines are also shown.

again a large improvement of the correlation coefficient, from 0.69 for the rain-normalized fluxes at the 33 stations to 0.79 for the geographically corrected fluxes. The mean bias is also significantly decreased from 8.9% to 0.4%.

4.4.3. Overall comparison. The comparison between observed and modeled fluxes after normalization by rainfall rate and geographical corrections is presented in Figures 10a and 10b for all stations of the northern and southern hemispheres, respectively. The observed deposition fluxes are generally well reproduced by the model, particularly in the southern hemisphere. For the northern hemisphere the greatest discrepancies appear in Greenland and northern Scandinavia where the model strongly overpredicts deposition fluxes. At Camp Century (77.18°N, 61.88°W) the deposition flux is overestimated by a factor of 5, with 50% of the annual flux occurring during the summer months. Looking at the predicted summer ^{210}Pb concentration in altitude over Thule (76.60°N, 65.58°W) shows a well-mixed column, whereas *Dibb et al.* [1992] report a threefold decrease from the surface to 5 km altitude in summer 1988 during the NASA Global Tropospheric Experiment/Arctic Boundary Layer Expeditions (GTE/ABLE 3A) mission. Moreover, we have already seen that the model overestimates the summer concentrations at the surface. The incapacity of the model to reproduce the vertical structure of the Greenland atmosphere could explain the very high tropospheric ^{210}Pb content and thus the overestimate in deposition flux.

Discrepancies of about a factor of 2 are also noticeable at some stations. The stations where it occurs are either experiencing the monsoon regime or located in elevated regions (indicated by arrows on Figure 10a). For elevated sites, *Graustein and Turekian* [1986] suggest that ^{210}Pb near the surface could be more efficiently removed due to orographically induced clouds [*Lovett et al.*, 1982].

Another source of incertitudes comes from the measurements themselves. Most of the observed deposition fluxes used in this study are bulk deposition fluxes. Some of them were measured via artificial collectors; others come from soil or snow samples [*Preiss et al.*, 1996]. To evaluate the influence of the measurements method on our comparison, we have compared observed and predicted deposition fluxes separately according to the collector used, the artificial one being the most accurate method. We have used the measurements in the United States and Europe, with 38 data measured in natural collectors and 29 in artificial collectors. The comparison has revealed that for the 38 stations where deposition fluxes were measured in soils, the mean bias is 4.1% with a correlation coefficient of 0.53. For the 29 other stations, although the mean bias is slightly increased to 7.3%, the correlation is significantly improved with r=0.91.

Finally, comparing the observed and modeled deposition fluxes at the 147 stations gives a mean bias of 1.2% and a correlation coefficient of 0.77. If we consider only the stations located below 900 m altitude, the correlation coefficient is increased to 0.85. Table 2 gives more information on this model-measure comparison of deposition fluxes. At 87% of the stations, predicted ^{210}Pb annual deposition fluxes agree with measurements within a factor of 2, and for about half of these stations, agreement between observed and simulated fluxes is better than 20%. This gives us good confidence in this parameterization of the scavenging of submicron particles in a global aerosol transport model.

5. Sensitivity Tests

5.1. Convective Rain Scavenging

We tested several parameters used in the parameterization of the wet removal of aerosol. The first tests were

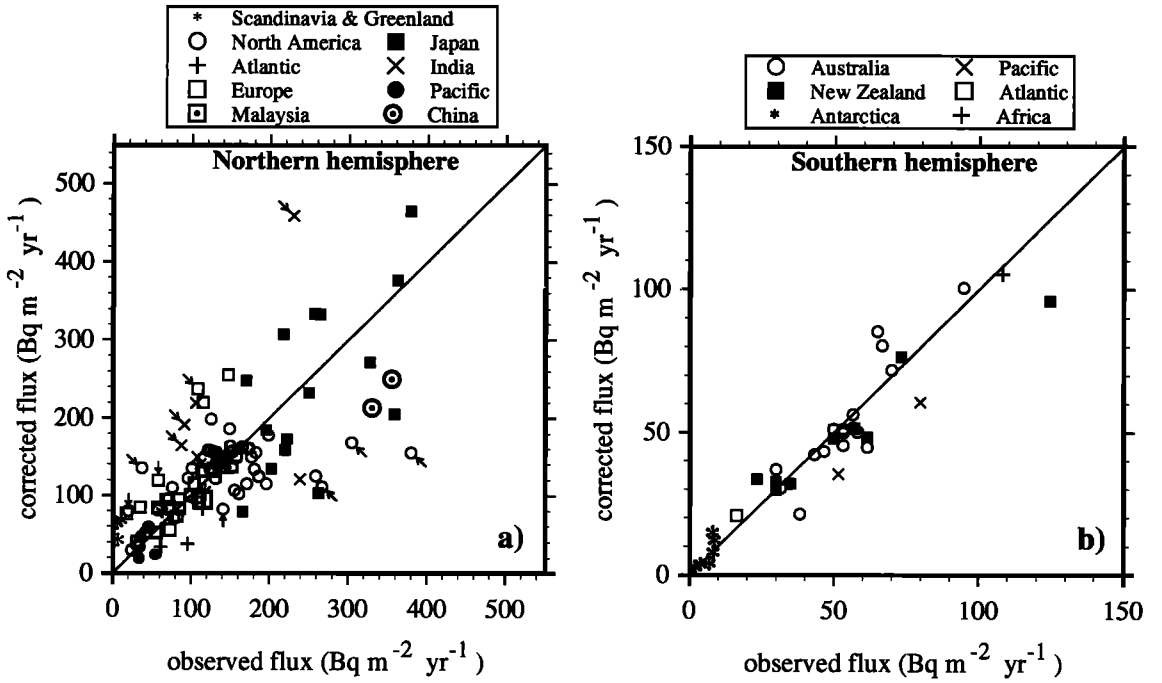

Figure 10. Comparison between observed and corrected (see text) annual total deposition flux of ^{210}Pb (Bq m^{-2} yr^{-1}) at the 147 stations for (a) northern and (b) southern hemispheres. Arrows indicate stations located above 900 m height. The 1:1 lines are also shown.

done on the scavenging efficiencies of 50% and 100% for the case of shallow and deep convective precipitation, respectively, which have been used in our reference simulation. As mentioned by *Balkanski et al.* [1993], decreasing the scavenging efficiency in deep convection events to 50% yields to an overestimate of the ^{210}Pb concentrations. For example, over the central Pacific the ^{210}Pb concentrations are increased by a factor of 2 at ground level, and by a factor of 3 at 6 km altitude, leading to an unrealistic ^{210}Pb atmospheric content.

On the other hand, increasing the scavenging efficiency in shallow convection to 100% affects especially surface air. Annual ^{210}Pb concentrations over midlatitude oceans decrease by 10 to 20%.

5.2. Stratiform Rain In-Cloud Scavenging

For the large-scale precipitation the parameters of importance are in-cloud and below-cloud scavenging efficiencies. In our scheme we consider that 100% of the aerosol present in the cloud is incorporated into cloud droplets. In situ measurements evaluated by *Schumann* [1989] show that for 15 rain events the in-cloud scavenging efficiency for particles of 0.37 μm diameter varies between 40% and 93%, with a mean value of 68%. These results agree with observations from *Hegg et al.* [1984], *Leaitch et al.* [1986], and *Gillani et al.* [1995], who report a mean value of 70%. Regardless of possible experimental difficulties, such variations for a specific particle size can be explained by the simultaneous effect of precipitation within the cloud (mostly in the ice phase), the presence of different proportions of soluble matter in the aerosol composition, and differing concentrations of very fine particles, which can compete in the particle activation process [*Leaitch et al.*, 1986; *Schumann* 1989; *Gillani et al.*, 1995]. To test the importance of this factor, we have made a ^{210}Pb simulation of July 1991 after a spin-up of 2 months with a 70% in-cloud scavenging efficiency. Absolute differences in deposition were less than ±8% at 90% of the sites. Differences in surface air concentrations are not important either. Had the aerosol originated from the high troposphere, these differences would be larger.

Table 2. Number of Stations (%) Lying Within a Given Bias Between Observed and Simulated Annual Deposition Flux

|Bias|, %	NH (112)	SH (35)	Global (147)
≤50	84%	97%	87%
≤40	74%	91%	78%
≤30	64%	77%	68%
≤20	45%	57%	49%
≤10	23%	46%	29%

Numbers in parentheses indicate the number of stations used. NH, northern hemisphere; SH, southern hemisphere.

5.3. Stratiform Rain Below-Cloud Scavenging

We have assumed that rainwater evaporation leads to a reduction of the raindrops diameter. We now examine this assumption. It is obvious that some of the raindrops will reduce until a critical diameter and completely evaporate, releasing their nucleated particle in the atmosphere. To assess the uncertainties linked to

our assumption, we have done simulations for January and July 1991 with a 2 months spin-up in which we release in the evaporating layer a fraction of the aerosol in rainwater equal to the fraction of this rainwater which evaporates.

In January, there is no noticeable change in the northern hemisphere. The tropospheric ^{210}Pb concentrations increase by 20% over the southern hemisphere oceans, with a peak increase of 50% in the low troposphere over the Indian and the Pacific Oceans poleward of 40°S where ^{210}Pb is scarce. This strong increase of ^{210}Pb concentrations is due to aerosol captured aloft which is released in the first kilometers near the ground as evaporation occurs. The agreement between observed and modeled ^{210}Pb surface concentrations deteriorates significantly at stations (the four Indian Ocean remote sites excepted) located below 30°S. Similar results are obtained in July.

Another source of uncertainty in computing wet scavenging is the value of the below-cloud scavenging coefficient. Integrating values of λ^* measured in situ by *Schumann* [1989] over the ^{210}Pb size distribution leads to a below-cloud coefficient of 0.8 cm^{-1} to be compared to 0.04 cm^{-1} calculated with the *Dana and Hales* [1976] parameterization. Results showed that increasing the below-cloud coefficient to 0.8 cm^{-1} leaves in-cloud scavenging the dominant process compared to below-cloud scavenging (below-cloud scavenging globally accounts for less than 2% of the total flux, with local maxima of 20%). It has therefore no large influence on a global scale for submicronic particles but becomes important for larger particles, such as mineral dust.

6. Conclusions

A wet-scavenging scheme has been incorporated into a global 3-D atmospheric transport model which fully describes the aerosol size distribution. This scheme separates the removal by convective precipitation from the removal by synoptic precipitation. Whereas the former is computed as part of the vertical air mass fluxes, we consider for the latter the vertical distribution of precipitation, and we compute independently in-cloud and below-cloud scavenging. Since wet removal below the cloud is dependent on particle size, we have used a parameterization which fully accounts for the aerosol size distribution. Sensitivity studies on the different parameters governing the wet scavenging in the model have highlighted the importance of distinguishing scavenging in shallow and deep convection to allow a realistic vertical redistribution of aerosols during convective events. During large-scale precipitation events, below-cloud scavenging has been found to be negligible for submicronic aerosols, whereas the accuracy of the in-cloud efficiency used in this study could not be constrained by the existing ^{210}Pb measurements.

To validate the wet deposition scheme, we have done a yearly simulation (1991) of ^{210}Pb, a submicronic aerosol which is principally removed from the atmosphere by precipitation. Monthly and yearly averaged surface air concentrations of ^{210}Pb from the model have been compared with measurements at 117 stations and modeled yearly total deposition fluxes of ^{210}Pb with measurements at 147 stations. The comparison between observed and modeled annual ^{210}Pb concentrations at the 117 stations has revealed a good estimate of the global ^{210}Pb atmospheric content, since the mean bias is negligible (-2.7%) and the correlation coefficient is 0.80. For stations located far from main continental sources the model reproduces very well the observed ^{210}Pb monthly concentrations, simulating both the annual mean and the seasonality. However, discrepancies between simulations and observations appear in some regions located near the sources, as well as over Indian Ocean. Improvements in the description of the PBL and the uncertainty in the ^{210}Pb source (or ^{222}Rn emissions) are likely to explain these problems.

Despite the nonlinearity between rainfall amount and resulting aerosol deposition, we have shown that the predicted ^{210}Pb deposition flux could be expressed as a linear function of the rainfall rate on a yearly mean. This allows to compare yearly averaged ^{210}Pb deposition fluxes from observations and from simulation when the annual predicted fluxes have been normalized by observed annual rainfall rates. We also have performed a geographical grid box selection for a number of coastal stations under marine influence. Results show that the model reproduces nicely annual deposition fluxes, since for 128 over 147 stations, annual deposition fluxes are predicted within a factor of 2. Considering all the stations, the mean bias is 1.2% and the correlation coefficient is 0.77. For elevated regions, the model is less appropriate, mainly because it does not account for scavenging by orographically induced clouds on the mountain slopes. Over Greenland the model does not capture characteristic transport over the ice sheet yielding to a strong overestimation of the observed fluxes. Unfortunately, this prevents us for estimating the deficiencies of the wet-scavenging scheme at these high latitudes, which does not account for scavenging by ice crystals and snow.

This study has permitted to estimate the accuracy of the model to reproduce observed ^{210}Pb deposition fluxes as well as surface concentrations. Despite the quality of the results obtained at the surface the model behavior with regard to the aerosol vertical distribution needs attention and will be presented in a follow-up paper (W. Guelle et al., Wet deposition in a global size-dependent aerosol transport model, 2, Influence of the wet-scavenging scheme on ^{210}Pb vertical profiles, surface concentrations and deposition, submitted to J. Geophys. Res.). We will also present the importance of an accurate wet scavenging parameterization by a comparison of our results with those obtained with two other wet deposition schemes commonly used in aerosol global simulations.

Appendix: Calculation of the Below-Cloud Scavenging Efficiency

The scavenging coefficient λ is defined as a first-order removal rate of the aerosol concentration c:

$$\left.\frac{dc}{dt}\right|_{\text{scav}} = -\lambda\, c \qquad \text{(A1)}$$

where λ can either be the in-cloud or the below-cloud scavenging coefficient. The associated scavenging efficiency η (no unit) can be defined for a time interval δt (s), or for a rainfall depth h (mm) within δt:

$$\eta = \frac{c(t) - c(t+\delta t)}{c(t)} = 1 - e^{-\lambda\,\delta t} = 1 - e^{-\lambda^* h} \qquad \text{(A2)}$$

where λ and λ^* are expressed in s^{-1} and mm^{-1}, respectively. *Dana and Hales* [1976] give a parameterization of λ^* according to the particle diameter d and integrate it over the aerosol size distribution [*Butcher and Charlson*, 1972] to calculate the scavenging coefficient Λ^* for a polydisperse aerosol. Because of the strong discontinuity of the function $\lambda^*(d)$ around 2 μm [see *García Nieto et al.*, 1994, Figure 2], this integration will induce an error on Λ^* (and thus on η) for size distributions including particles in this size range, as for mineral dust and sea salts. We have computed this error on η for several mean diameters of dust size distributions ($\sigma = 1.9$, ρ_p=2.65 g cm^{-3}). It is of 30% for MMD=1.5 μm and a rain amount of 2 mm, of 45% for MMD=1.3 μm and a rain amount of 3 mm, and of 80% for MMD=1 μm and a rain amount of 7 mm. We therefore chose to precalculate for a given aerosol (characterized by ρ_p and σ) the scavenging efficiencies in a more accurate way:

$$\eta(\text{MMD}, h) = \sum_{i=1}^{n} \left[1 - e^{-\lambda^*(d_i)\,h}\right] c(d_i) \qquad \text{(A3)}$$

where $c(d_i)$ is the relative contribution of particles with diameter d_i to the total aerosol mass (or particles number). The concentration $c(d_i)$ is shared on the size range 10^{-6}-10^{3} μm in $n = 10^4$ logarithmically spaced bins according to the size distribution parameters (MMD and σ). We have tabulated different values of η according to the different parameters (MMD, h) provided at each time step by the model in order to save computing time.

Acknowledgments. We are grateful to Stefan Rehfeld for providing us with the formatted files of measurement data. We also want to thank Nicolas Preiss and Marie-Antoinette Mélières for granting us an early access to the large ^{210}Pb database they have assembled. This work was partly supported by the German-French cooperation fund PROCOPE and the EU-Environment & Climate Project SINDICATE (contract ENV4-CT95-0099). This is LSCE contribution 42.

References

Arimoto R., R. A. Duce, B. J. Ray, and C. K. Unni, Atmospheric trace elements at Enewetak Atoll, 2, Transport to the ocean by wet and dry deposition, *J. Geophys. Res., 90,* 2391-2408, 1985.

Balkanski, Y. J., D. J. Jacob, G. M. Gardner, W. C. Graustein, and K. K. Turekian, Transport and residence times of tropospheric aerosols inferred from a global three-dimensional simulation of ^{210}Pb, *J. Geophys. Res., 98,* 20,573-20,586, 1993.

Bondietti, E. A., C. Papastefanou, and C. Rangarajan, Aerodynamic size associations of natural radioactivity with ambient aerosols, in *Radon and Its Decay Products: Occurrence, Properties, and Health Effects, ACS Symp. Ser.*, vol. 331, edited by P.K. Hopke, pp. 377-397, Am. Chem. Soc., Washington, D. C., 1987.

Bondietti, E. A., J. N. Brantley, and C. Rangarajan, Size distributions and growth of natural and Chernobyl-derived submicron aerosols in Tennessee, *J. Environ. Radioact., 6,* 99-120, 1988.

Brost, R. A., and R. B. Chatfield, Transport of radon in a three-dimensional subhemispheric model, *J. Geophys. Res., 94,* 5095-5119, 1989.

Butcher, S. S., and R. J. Charlson, An Introduction to Air Chemistry, pp 167-171, Academic, San Diego, Calif., 1972.

Charlson, R. J., S. E. Schwartz, J. M. Hales, R. D. Cess, J. A. Coakley Jr., J. E. Hansen, and D. J. Hofmann, Climate forcing by anthropogenic aerosols, *Science, 255,* 423-430, 1992.

Chiapello, I., G. Bergametti, L. Gomes, and B. Chatenet, An additional low layer transport of Sahelian and Saharan dust over the North-Eastern Tropical Atlantic, *Geophys. Res. Lett., 22,* 3191-3194, 1995.

Chin, M., D. J. Jacob, G. M. Gardner, M. S. Foreman-Fowler, and P. A. Spiro, A global three-dimensional model of tropospheric sulfate, *J. Geophys. Res., 101,* 18,667-18,690, 1996.

Commissariat à l'Energie Atomique (CEA), Synthèse mensuelle des mesures de radioactivité effectuées dans l'environnement du groupe CEA, *Reps. DPS 90/001/3, DPS 90/001/4, DPS 90/001/5,* Dép. de Prot. Sanit., France, 1990.

Cooke, W. F., and J. J. N. Wilson, A global black carbon aerosol model, *J. Geophys. Res., 101,* 19,395-19,409, 1996.

Dana, M. T., and J. M. Hales, Statistical aspects of the washout of polydisperse aerosols, *Atmos. Environ., 10,* 45-50, 1976.

Dibb, J. E., R. W. Talbot, and G. L. Gregory, ^{7}Be and ^{210}Pb in the western hemisphere arctic atmosphere: Observations from the three recent aircraft-based sampling programs, *J. Geophys. Res., 97,* 16,709-16,715, 1992.

Dörr, H., and K. O. Münnich, ^{222}Rn flux and soil air concentration profiles in West-Germany. Soil ^{222}Rn as tracer for gas transport in the unsaturated soil zone, *Tellus, Ser. B, 42,* 20-28, 1990.

Dulac, F., P. Buat-Ménard, U. Ezat, S. Melki, and G. Bergametti, Atmospheric input of trace metals to the western Mediterranean: Uncertainties in modeling dry deposition from cascade impactor data, *Tellus, Ser. B, 41,* 363-378, 1989.

Ehhalt, D. H., Turnover times of ^{137}Cs and HTO in the troposphere and removal rates of natural aerosol particles and water vapor, *J. Geophys. Res., 78,* 7076-7086, 1973.

Feichter, J., and P. J. Crutzen, Parameterization of vertical tracer transport due to deep cumulus convection in a global transport model and its evaluation with ^{222}Rn measurements, *Tellus, Ser. B, 42,* 100-117, 1990.

Feichter, J., R. A. Brost, and M. Heimann, Three-dimensional modeling of the concentration and deposition of ^{210}Pb aerosols, *J. Geophys. Res., 96,* 22,447-22,460, 1991.

Feichter, J., E. Kjellstrom, H. Rodhe, F. Dentener, J. Lelieveld, and G.-J. Roelofs, Simulation of the tropospheric sulfur cycle in a global climate model, *Atmos. Environ., 30,* 1693-1708, 1996.

García Nieto, P. J., B. Arganza García, J. M. Fernández Díaz, and M. A. Rodríguez Braña, Parametric study of selective removal of atmospheric aerosol by below-cloud scavenging, *Atmos. Environ., 28,* 2235-2342, 1994.

Genthon, C., Simulations of desert dust and sea-salt aerosols in Antarctica with a general circulation model of the atmosphere, *Tellus, Ser. B, 44,* 371-389, 1992.

Gillani, N. V., S. E. Schwartz, W. R. Leaitch, J. W. Strapp, and G. A. Isaac, Field observations in continental stratiform clouds: Partitioning of cloud particles between droplets and unactivated interstitial aerosols, *J. Geophys. Res., 100,* 18,687-18,706, 1995.

Giorgi, F., and W. L. Chameides, Rainout lifetimes of highly soluble aerosols and gases as inferred from simulations with a general circulation model, *J. Geophys. Res., 91,* 14,367-14,376, 1986.

Gopalakrishnan, S., C. Rangarajan, L. U. Joshi, D. K. Kapoor, and C. D. Eapen, Measurements on airborne and surface fallout radioactivity in India, Gov. of India, At. Energy Comm., Bhabha At. Res. Cent., Bombay, 1973.

Graustein, W. C., and K. K. Turekian, ^{210}Pb and ^{137}Cs in air and soils measure the rate and vertical profile of aerosol scavenging, *J. Geophys. Res., 91,* 14,355-14,366, 1986.

Hegg, D. A., P. V. Hobbs, and L. F. Radke, Measurements of the scavenging of sulfate and nitrate in clouds, *Atmos. Environ., 18,* 1939-1946, 1984.

Heimann, M., The global atmospheric model TM2, *Tech. Rep. 10,* Dtsch. Klimarechenzent., Modellbetreuungsgruppe, Hamburg, Germany, 1995.

Heimann, M., and C. D. Keeling, A three-dimensional model of atmospheric CO_2 transport based on observed winds, 2, Model description and simulated tracer experiments, *Geophys. Monogr. Ser., 55,* 237-275, 1989.

Husar, R. B., J. M. Prospero, and L. L. Stowe, Characterization of tropospheric aerosols over the oceans with the NOAA advanced very high resolution radiometer optical thickness operational product, *J. Geophys. Res., 102,* 16,889-16,909, 1997.

International Panel on Climate Change (IPCC), *Climate Change 1994: Radiative Forcing of Climate Change,* edited by J.T. Houghton, L.G. Meira Filho, J. Bruce, Hoesung Lee, B.A. Callander, E. Haites, N. Harris, and K. Maskell, Cambridge University Press, New York, 1994.

Jacob, D. J., and M. J. Prather, ^{222}Rn as a test of boundary layer convection in a general circulation model, *Tellus, Ser. B, 42,* 118-134, 1990.

Jacob, D. J., M. J. Prather, P. J. Rasch, R.-L. Shia, et al., Evaluation and intercomparison of global atmospheric transport models using ^{222}Rn and other short-lived tracers, *J. Geophys. Res., 102,* 5953-5970, 1997.

Joshi, L. U., C. Rangarajan, and S. Gopalakrishnan, Measurement of ^{210}Pb in surface air and precipitation, *Tellus, Ser. B, 21,* 107-112, 1969.

Joussaume, S., Three-dimensional simulations of the atmospheric cycle of desert dust particles using a general circulation model, *J. Geophys. Res., 95,* 1909-1941, 1990.

Kiehl, J. T., and B. P. Briegleb, The relative roles of sulfate aerosols and greenhouse gases in climate forcing, *Science, 260,* 311-314, 1993.

Knuth, R. H., E. O. Knutson, H. W. Feely, and H. L. Volchok, Size distributions of atmospheric Pb and ^{210}Pb in rural New Jersey: Implications for wet and dry deposition, in *Precipitation Scavenging, Dry Deposition, and Resuspension,* vol. 2, pp. 1325-1335, Elsevier Sci., New York, 1983.

Kolb, W., Radionuclide concentrations in ground-level air from 1980 to 1983 in north Germany and north Norway, *Ber. Ra-15,* Phys.-Tech. Bundesanst., Braunschweig, Germany, 1984.

Kolb, W., Radionuclide concentrations in ground-level air from 1984 to mid 1986 in north Germany and north Norway: Influence of the Chernobyl accident, *Ber. Ra-18,* Phys.-Tech. Bundesanst., Braunschweig, Germany, 1986.

Kolb, W., Radionuclide concentrations in ground-level air from 1986 to 1987 in north Germany and north Norway, *Ber. PTB-Ra-21,* Phys.-Tech. Bundesanst., Braunschweig, Germany, 1988.

Kolb, W., Radionuclide concentrations in ground-level air from 1988 to 1989 in north Germany and north Norway, *Ber. PTB-Ra-25,* Phys.-Tech. Bundesanst., Braunschweig, Germany, 1990.

Kritz, M. A., J.-C. Le Roulley, and E. F. Danielsen, The China Clipper–fast advective transport of radon-rich air from the Asian boundary layer to the upper troposphere near California, *Tellus, Ser. B, 42,* 46-61, 1990.

Lambert, G., G. Polian, J. Sanak, B. Ardouin, A. Buisson, A. Jegou, and J.-C. Le Roulley, Cycle du radon et de ses descendants: Application à l'étude des échanges troposphère-atmosphère, *Ann. Geophys., 38,* 497-531, 1982.

Lambert, G., B. Ardouin, and J. Sanak, Atmospheric transport of trace elements toward Antarctica, *Tellus, Ser. B, 42,* 76-82, 1990.

Langner, J., and H. Rodhe, A global three-dimensional model of the tropospheric sulfur cycle, *J. Atmos. Chem., 13,* 225-263, 1991.

Larsen, R. J., C. G. Sanderson, and J. Kada, EML surface air sampling program, 1990-1993 data, *Rep. EML-572,* Environ. Meas. Lab., U.S. Dep. of Energy, New York, 1995.

Leaitch, W. R., J. W. Strapp, G. A. Isaac, and J. G. Hudson, Cloud droplet nucleation and scavenging of aerosol sulphate in polluted atmospheres, *Tellus, Ser. B, 38,* 328-344,1986.

Lee, H. N., and J. Feichter, An intercomparison of wet precipitation scavenging schemes and the emission rates of ^{222}Rn for the simulation of global transport and deposition of ^{210}Pb, *J. Geophys. Res., 100,* 23,253-23,270, 1995.

Liousse, C., J. E. Penner, C. Chuang, J. J. Walton, H. Eddleman, and H. Cachier, A global three-dimensional model study of carbonaceous aerosols, *J. Geophys. Res., 101,* 19,411-19,432, 1996.

Louis, J. F., A parametric model of vertical eddy fluxes in the atmosphere, *Boundary Layer Meteorol., 17,* 187-202, 1979.

Lovett, G. M., W. A. Reiners, and R. K. Olson, Cloud droplet deposition in subalpine balsam fir forests: Hydrological and chemical inputs, *Science, 218,* 1303-1304, 1982.

Mahowald, N. M., P. J. Rasch, and R. G. Prinn, Cumulus parameterizations in chemical transport models, *J. Geophys. Res., 100,* 26,173-26,189, 1995.

Mattson, R., Seasonal variation of short-lived radon progeny, ^{210}Pb and ^{210}Pb ^{210}Po , in ground level air in Finland, *J. Geophys. Res., 75,* 1741-1744, 1970.

Nho, E.-Y., B. Ardouin, M.-F. Le Cloarec, and M. Ramonet, Origins of ^{210}Po in the atmosphere at Lamto, Ivory Coast: Biomass burning and Saharan dusts, *Atmos. Environ., 30,* 3705-3714, 1996.

Penner, J. E., S. J. Ghan, and J. J. Walton, The role of biomass burning in the budget and cycle of carbonaceous

soot aerosols and their climate impact, in *Global Biomass Burning*, edited by J.S. Levine, pp. 387-393, MIT Press, Cambridge, Mass., 1991.

Penner, J. E., R. E. Dickinson, and C. A. O'Neill, Effects of aerosol from biomass burning on the global radiation budget, *Science, 256*, 1432-1434, 1992.

Pham, M., J.-F. Müller, G. Brasseur, C. Granier, and G. Mégie, A three-dimensional study of the tropospheric sulfur cycle, *J. Geophys. Res., 100*, 26,061-26,092, 1995.

Polian, G., G. Lambert, B. Ardouin, and A. Jegou, Long-range transport of continental radon in subantarctic and antarctic area, *Tellus, Ser. B, 38*, 178-189, 1986.

Prakasa Rao, P. S., L. T. Khemani, G. A. Momin, P. D. Safai, and A.G. Pillai, Measurements of wet and dry deposition at an urban location in India, *Atmos. Environ., 26*, 73-78, 1992.

Preiss, N., M.-A. Mélières, and M. Pourchet, A compilation of data on ^{210}Pb concentration in surface air and fluxes at the air-surface and water-sediment interfaces, *J. Geophys. Res. 101*, 28,847-28,862, 1996.

Rahn, K. A., and R. J. McCaffrey, On the origin and transport of the winter arctic aerosol, *Ann. N.Y. Acad. Sci., 388*, 486-503, 1980.

Ramonet, M., Variabilité du CO_2 atmosphérique en régions australes: Comparaison modèle/mesures, 295 pp., Thèse de Sciences, Univ. Paris VII, 1994.

Ramonet, M., and P. Monfray, CO_2 baseline concept in 3-D atmospheric transport models, *Tellus, Ser. B, 48*, 502-520, 1996.

Rehfeld, S., and M. Heimann, Three-dimensional atmospheric transport simulation of the radioactive tracers ^{210}Pb , ^{7}Be, ^{10}Be, ^{90}Sr, *J. Geophys. Res., 100*, 26,141-22,161, 1995.

Russell, G. L., and J. A. Lerner, A new finite-differencing scheme for the tracer transport equation, *J. Appl. Meteorol., 20*, 1483-1498, 1981.

Sanak, J., A. Gaudry, and G. Lambert, Size distribution of ^{210}Pb aerosols over oceans, *Geophys. Res. Lett., 8*, 1067-1070, 1981.

Schneider, J. K., R. B. Gagosian, J. K. Cochran, and T. W. Trull, Particle size distributions of *n*-alkanes and ^{210}Pb in aerosols off the coast of Peru, *Nature, 304*, 429-432, 1983.

Schulz, M., Y. J. Balkanski, F. Dulac, and W. Guelle, Role of aerosol size distribution and source location in a 3D simulation of a Saharan dust episode tested against satellite-derived optical thickness, *J. Geophys. Res.*, in press, 1997.

Schumann, T., Precipitation scavenging of aerosol particles: A wintertime field study, 293 pp., Ph.D. thesis, Swiss Fed. Inst. of Technol. (ETH), Zürich, 1989.

Sokolik, I. N., and O. B. Toon, Direct radiative forcing by anthropogenic airborne mineral aerosols, *Nature, 381*, 681-683, 1996.

Tegen, I., and I. Fung, Modeling of mineral dust in the atmosphere: Sources, transport, and optical thickness, *J. Geophys. Res., 99*, 22,897-22,914, 1994.

Tegen I., and A. A. Lacis, Modeling of particle size distribution and its influence on radiative properties of mineral dust aerosol, *J. Geophys. Res., 101*, 19,237-19,244, 1996.

Tegen I., A. A. Lacis, and I. Fung, The influence on climate forcing of mineral aerosols from disturbed soils, *Nature, 380*, 419-422, 1996.

Tiedtke, M., A comprehensive mass flux scheme for cumulus parameterization in large-scale models, *Mon. Weather Rev., 117*, 1779-1800, 1989.

Todd, J. F., and G. T. F. Wong, Atmospheric depositional characteristics of ^{7}Be and ^{210}Pb along the southeastern Virginia coast, *J. Geophys. Res., 94*, 11,106-11,116, 1989.

Tsunogai, S., T. Shinagawa, and T. Kurata, Deposition of anthropogenic sulfate and ^{210}Pb in the western North Pacific area, *Geochem. J., 19*, 77-90, 1985.

Tsunogai, S., T. Kurata, T. Suzuki, and K. Yokota, Seasonal variation of atmospheric ^{210}Pb and Al in the western North Pacific region, *J. Atmos. Chem., 7*, 389-407, 1988.

Turekian, K. K., Y. Nozaki, and L. K. Benninger, Geochemistry of atmospheric radon and radon products, *Ann. Rev. Earth Planet. Sci., 5*, 227-255, 1977.

Turekian, K. K., W. C. Graustein, and J. K. Cochran, ^{210}Pb in the SEAREX program: An aerosol tracer across the Pacific, in *Chemical Oceanography*, vol. 10, edited by J.P. Riley and R. Chester, pp. 51-81, Academic, San Diego, Calif., 1989.

Uematsu, M., R. A. Duce, and J. M. Prospero, Deposition of atmospheric mineral particles in the North Pacific Ocean, *J. Atmos. Chem., 3*, 123-138, 1985.

Wilkening, M. H., and W. E. Clements, ^{222}Rn from the ocean surface, *J. Geophys. Res., 80*, 3828-3830, 1975.

Y. J. Balkanski (corresponding author) and W. Guelle, Laboratoire des Sciences du Climat et de l'Environnement, Commissariat à l'Energie Atomique, Centre d'Etudes de Saclay, L'Orme des Merisiers 709, F-91191 Gif-sur-Yvette Cedex, France. (e-mail: balkansk@lsce.saclay.cea.fr; guelle@lsce.saclay.cea.fr)

F. Dulac and P. Monfray, Centre des Faibles Radioactivités, Centre National de la Recherche Scientifique - Commissariat à l'Energie Atomique, F-91198 Gif-sur-Yvette Cedex, France. (e-mail: dulac@lsce.saclay.cea.fr; monfray@lsce.saclay.cea.fr)

M. Schulz, Institut für Anorganische und Angewandte Chemie, Universität Hamburg, Martin-Luther-King-Platz 6, D-20146 Hamburg, Germany. (e-mail: michael.schulz@dkrz.de)

(Received June 17, 1997; revised December 5, 1997; accepted December 10, 1997.)